Discovery and Recovery of delta *p*-aminobenzoic acid

Martin R. Ward,[1] Shatha Younis,[1] Aurora J. Cruz-Cabeza,[2] Craig L. Bull,[3] Nicholas P. Funnell,[3] and Iain D.H. Oswald[1]

[1] Strathclyde Institute of Pharmacy & Biomedical Sciences (SIPBS), University of Strathclyde, 161 Cathedral Street, G4 0RE, Glasgow, U.K.

[2] School of Chemical Engineering and Analytical Science, University of Manchester, M13 9PL Manchester, United Kingdom

[3] ISIS Neutron and Muon Source, Science and Technology Facilities Council, Rutherford Appleton Laboratory, Harwell, Didcot, OX11 0QX, UK

Abstract

We explore the polymorphism of p-aminobenzoic acid (*p*ABA) under high-pressure conditions. We have been able to isolate a new high-pressure form (δ-*p*ABA) at pressures exceeding 0.3 GPa from three different pressure-transmitting media, water, water:ethanol and pure ethanol. We explore the compression behaviour of α-*p*ABA in each of these media using neutron powder diffraction and observe that the transition is kinetically hindered using the aqueous ethanol and ethanol solutions compared with the pure aqueous medium. δ-*p*ABA is sufficiently stable to be recovered to ambient pressure to enable its characterisation via X-ray powder diffraction and differential scanning calorimetry. At ambient pressure we have observed that δ-*p*ABA converts into α-*p*ABA on heating beyond 70 °C.

Keywords: p-aminobenzoic acid, neutron powder diffraction, high pressure, recovery

Introduction

The discovery of and relationships between different solid-state forms of molecular materials is of paramount importance to industry due to the changes in physicochemical properties that may exist between phases.[1] The nucleation of specific polymorphs of a pharmaceutical, for example, can be initiated through seeding experiments to ensure that the correct polymorph is isolated from a crystallisation. From that point on, the behaviour of the solid is assumed to be well controlled and hence the ability to process into a formulated product can be achieved. However, at every stage of the operation there is the possibility of transformation of the desired polymorph into a new, as yet, unidentified polymorph that can cause issues in the formulated product.[2]

To explore the solid-state landscape fully we need to be able to probe both the thermodynamic variables of temperature and pressure. The investigation of solid-state

polymorphs using temperature has become routine with the advent of variable temperature devices for analytical equipment such as calorimetry and diffraction.[3–5] Whilst significant improvements and developments of both hardware and software have been made, which permit laboratory based characterisation of the effects of pressure, there are still relatively few such studies reported to date.[6–17] Phase transformations of organic materials at high pressure can potentially be observed by purely compressing materials into new forms via a single crystal-to-single crystal mechanism,[18–23] or through reconstructive mechanisms that result in the degradation of the crystals.[24,25] The characterisation of the latter can prove challenging, however, depending on the pressure at which the transition occurs, one can use a solution of the material and perform a recrystallisation at high pressure. This method has been used to facilitate the growth of single crystals of these degraded samples for single crystal X-ray diffraction measurement.[11,26]

Para-aminobenzoic acid (*p*ABA) has three polymorphs and has been the subject of numerous crystallisation studies at various temperatures.[27–35] For a more comprehensive review of *p*ABA polymorphism readers are directed to the article by Cruz-Cabeza et al. following this one.{REF TO BE PROVIDED ONCE DOI ASSIGNED} Its simple molecular structure provides a rich phase behaviour that signifies the potential for the discovery of new phases at high pressure. Yan *et al* investigated the pressure dependence of α- and β-*p*ABA (both $P2_1/n$) observing that both phases are stable to 13 GPa using an inert pressure-transmitting medium, silicone oil.[36] Through *ab initio* approaches they calculated the compression of the crystal structure assuming there was no change in phase and attributed the stability of the polymorphs to the hydrogen bonded dimers and tetramers in α-*p*ABA and β-*p*ABA respectively. Following this work, we wanted to explore how *p*ABA would react to compression using different pressure transmitting media in which the solubility of *p*ABA varied from low (water) to high (ethanol). In the following paper we describe the crystallisation behaviour using neutron diffraction and spectroscopic techniques.

Methods

Sample preparation

p-Aminobenzoic acid (*p*ABA; purity 99%, Sigma-Aldrich A9878; LOT MKBZ3723V) was used to prepare individual samples prior to loading Diamond Anvil cells. An excess of *p*ABA was weighed in 1ml of the selected solvent (water; 50:50 water:ethanol; ethanol) and stirred for approximately 2-4 hours

at room temperature (293 K). The solution was filtered into a new vial using a 0.2 μm filter, prior to loading the cells.

High pressure

A Merrill- Bassett Diamond Anvil Cell (DAC)[37] was equipped with two Boehler-Almax gem-diamonds with culets of 600 μm seated in tungsten carbide backing discs. A 250 μm hole was drilled in a pre-indented tungsten gasket with a thickness of 90 μm using a Boehler-Almax microdriller. Small pieces of ruby were loaded into the sample chamber to act as a pressure calibrant.[38] For the compression studies a powdered sample of *p*ABA was added to the sample chamber along with a drop of the pre-prepared solution described above.

For the recrystallisation experiments using ethanol or the water:ethanol mixture a saturated solution was added to the DAC together with a piece of ruby (to act as a pressure marker by the standard fluorescence method).[39] No further addition of solid material was required as there was enough solute in the solution to allow precipitation on application of pressure. In the case of water, the solubility of *p*ABA was low enough that a small crystallite of α-*p*ABA was required along with the saturated solution so that on precipitation at pressure there was enough sample for analysis by X-ray diffraction. At each pressure point (Ethanol: 0.22 and 0.49 GPa; mixture: 0.8 and 1.2 GPa; water: 0.27, 0.33 and 0.71 GPa), the cell was heated to dissolve the small crystallite and subsequently cooled to allow the precipitation. In some instances, pressure-cycling was required to initiate precipitation. Once a solid material appeared the temperature was cycled from room temperature to 323 K so as to anneal the small crystallites into one singular crystal or only a few smaller crystals that were in different orientations providing the potential for extra data given the limited access via the pressure cell.

Raman spectroscopy

A Horiba Xplora Raman Microscope from Horiba Scientific John Yvon coupled with a 532nm excitation laser was used to measure the Raman spectra of the samples at high pressure. Slit, hole, filters and accumulation times were varied to maximise the sample signal and reduce any fluorescence that may have come from the sample environment.

Infrared Spectroscopy

Fourier Transform Infrared spectroscopy (FT-IR) data was collected using a Bruker Tensor-II spectrometer equipped with a DigiTect 24 Bit ADC detectors. For each spectrum 16 scans were performed with a resolution of 4 cm^{-1} over the range 400-4000 cm^{-1}.

Differential scanning calorimetry

Differential Scanning Calorimetry (DSC) data was collected using a Netzsch DSC 214 Polyma calibrated for both temperature and sensitivity over the temperature range -93°C to 605°C, at a heating

rate of 20°C min^{-1} using thermal standards (indium, tin, bismuth and zinc) supplied by Netzsch. Approximately 6 mg of sample material was weighed into pre-weighed aluminium pans before sealing with a pierced lid. Samples were subject to 2 heating and cooling cycles from 20 to 200 °C at a rate of 20 °C min^{-1}. A 5-minute isothermal hold was programmed after each heat and cool step. The furnace was purged with helium (60 mL min^{-1}) during the experiments.

Single Crystal X-ray Diffraction.

Single crystal data were collected on a Bruker D8 Venture diffractometer equipped with an Incoatec IμS microfocussed Cu X-ray source ($K\alpha_1$ = 1.5406 Å). Suitable crystals were identified and mounted on a low-background Kapton microloop (200 μm). Crystals were indexed using a fast scan experimental method from which the collection strategy was determined using Bruker Apex3 software. Scaling[40] and data reduction were also performed using Apex3 software. For low-temperature analysis, data were collected at 100 K using an Oxford Cryostream cooling system.[41] Structures were solved by intrinsic phasing using ShelXT[42] through Olex2 (v1.2)[43] software. Full matrix least-squares refinement of data was also performed using Olex2 with ShelXL. All non-hydrogen atoms were treated anisotropically. Hydrogen atoms were placed geometrically (followed by a positional refinement for the acidic/amine hydrogens) and were subsequently constrained to ride on their parent atoms.

High-pressure diffraction data were collected on a Bruker APEX2 diffractometer equipped with an Incoatec IμS microfocussed Mo X-ray source ($K\alpha_1$ = 0.71073 Å). Data collection procedures followed those of Dawson et al.[44] with the addition of four runs at χ = 90°. The data were reduced in APEX3 using the dynamic masking procedures implemented in the software. Absorption corrections were applied using SADABS[40] as implemented in the Scale function in APEX3. Ambient pressure structures were used as the starting models for the refinements using Olex2.[43] RIGU restraints were used to aid the modelling of the displacement parameters. Hydrogen atoms were placed geometrically and allowed to refine before riding constraints were applied.

Neutron powder diffraction

High-pressure neutron powder diffraction data were collected for *p*ABA-d^4 (CDN isotopes, #D4209, lot #X-496) using the *PEARL* diffractometer[45] at the ISIS spallation neutron source located at the STFC Rutherford Appleton Laboratory. Three experiments were conducted with different pressure-transmitting media. The sample was ground and placed into a standard Ti-Zr alloy encapsulated gasket.[46] The media was added dropwise to the sample to provide quasi-hydrostatic conditions during the compression. A lead pellet (~80 mg) was added to the gasket to act as a suitable pressure marker. The resulting capsule assembly was then compressed within a type *V3b* Paris-Edinburgh (P-E) press[27] equipped with standard profile anvils with cores fabricated from zirconia toughened alumina (ZTA). The P-E cell piston pressure was monitored and controlled by means of an automated hydraulic system. For the pure D_2O system we observed poor wetting of

the solid during initial attempts at loading the sample. A successful loading was performed where the *p*ABA-d^4 sample was loaded with a pellet of frozen D_2O. The D_2O melted within the timeframe of loading the press onto the diffractometer which was confirmed through the lack of ice peaks in the diffraction patterns.

Time-of-flight (TOF) neutron powder diffraction data suitable for Pawley refinement were collected and the diffraction pattern intensities were corrected for the wavelength and scattering-angle dependence of the neutron attenuation by the P-E cell anvil and gasket (Ti-Zr) materials.[45,47] Sample pressures were calculated from the refined lead lattice parameters and the known equation of state.

Each sample was compressed and data were collected at regular intervals to a maximum pressure of 1.104(9) GPa (D_2O) and ~2 GPa (EtOD:D_2O; EtOD). In general, data were collected at each pressure point for 30-60 minutes with longer collections at the maximum pressure (2 hrs). For all samples, data were collected at various pressures on decompression (EtOD: 0.38 GPa, ambient; EtOD:D_2O: 1.57, 1.46, 0.94, 0.89, 0.64, 0.02 GPa, ambient; D_2O: only ambient). The final ambient pressure collection was to observe the recovery of the high-pressure phase.

Large volume press

A large volume press (LVP) was used to prepare δ-*p*ABA-h^7 at University of Strathclyde.[48] The starting material was identified as α-*p*ABA by X-ray powder diffraction (XRPD). The material was lightly ground before loading ca. 300 mg in to a polytetrafluoroethylene (PTFE) sample chamber that was comprised of a cylindrical tube (ID = 8mm, OD = 10mm) the ends of which were sealed using PTFE caps and PTFE sealing tape. The remaining volume of the sample chamber was filled with a saturated aqueous *p*ABA solution (298 K). The PTFE sample chamber was transferred to the large volume press cell assembly and a maximum load of 7 tonnes was applied to the sample (equivalent pressure = 0.8 GPa). The sample was held at elevated pressure conditions for a period of *ca.* 16 hours. Over the course of the 16 hours, the load on the sample had decreased to 6 tonnes (P = 0.69 GPa) indicating a loss of pressure over the time period. Sample solids were rapidly isolated from the aqueous solution by filtration. During filtration it was noted that the recovered sample was comprised of well-defined crystals with a pink hue. Recovered samples were stored in a sealed container prior to analysis. The samples were characterized by means of X-ray diffraction (SC-XRD and XRPD), Raman, FT-IR and DSC.

Results and Discussion

Single crystal diffraction

We investigated *p*ABA using the established recrystallisation at high-pressure methodology where a saturated solution of solute in a solvent system is loaded into a pressure vessel and pressure

applied to induce crystallisation.[49,50] The morphology of α-*p*ABA is a distinctive needle shape compared with the prism and block morphology of β- and γ-forms,[34] respectively. Hence, we would have indications of new solid forms depending on the morphology of the crystals grown at pressure. The γ-form has also been identified as needles which makes the separation from the α-form difficult.[32] Through sequential application of pressure and heating, we were able to observe the growth of the crystals and their morphology with subsequent identification using single-crystal X-ray diffraction. From all three media block-like crystals were isolated at pressures beyond 0.3 GPa (Table ES1). These crystals were indexed as a new monoclinic phase (*Pn*, *Z*' = 1) which we will designate as δ-*p*ABA. δ-*p*ABA has a similar packing as β-*p*ABA with a perpendicular hydrogen bonding arrangement between the acid group and the amine to form chains along the [1 0 1] direction (Figure 1b), however it is the interchain interaction that differs. In δ-*p*ABA, the neighbouring π-stacked molecule is orientated in the same direction whilst the molecules are anti-parallel in the β-polymorph. The parallel chains are linked to each other through the amine hydrogen bond to the carbonyl moiety of the acid group. The second hydrogen on the amine remains unfulfilled indicating the packing of molecules is of paramount importance rather than the fulfilment of the hydrogen bonding groups.

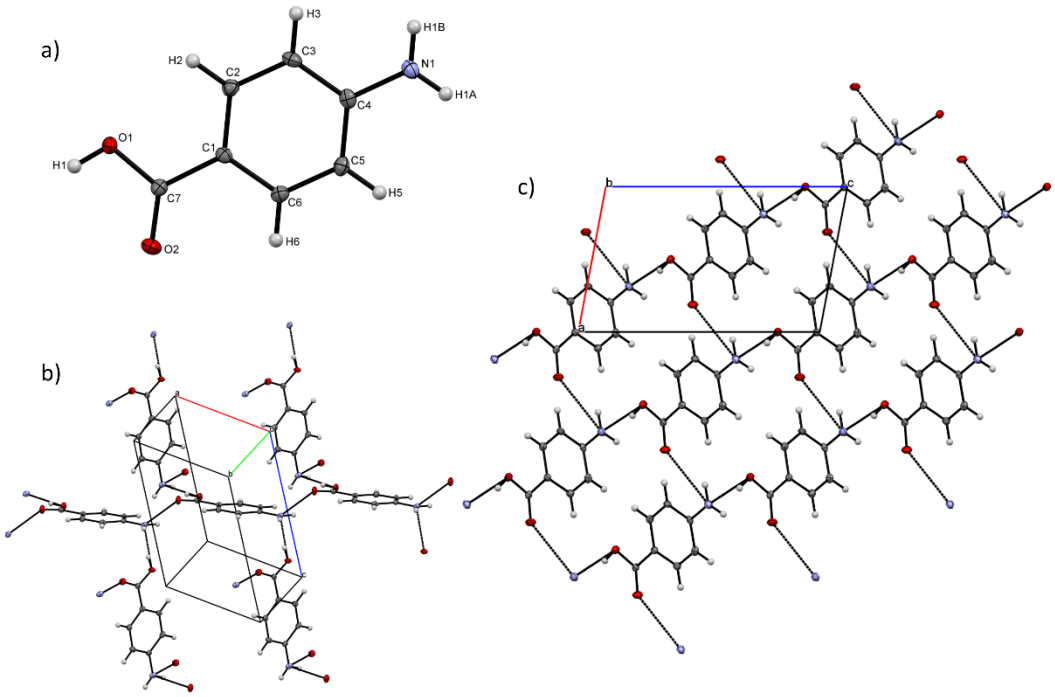

Figure 1: a) the numbering scheme for *p*ABA; b) the amine-carboxylic acid hydrogen bond forms 'head-to-tail' chains (central three molecules) whilst the carboxylic acid hydrogen bonds to the amine in a perpendicular interaction between neighbouring molecules (vertical interactions); and c) the packing of the δ-phase viewed down the *b*-axis.

Compression of saturated solutions to obtain the δ-polymorph led to the inevitable issue of dissolution of the sample on decompression. To overcome this problem we began to explore the effect of the solute/solution properties on the behaviour of *p*ABA under high pressure conditions with a view that the increase in solubility in the pressure-transmitting medium may overcome the kinetic barriers to interconversion. Previous work on the α- and β-forms at high pressure using Raman spectroscopy indicated that each of the phases were stable on compression to 13 GPa.[36] The stability of the α- and β-forms was attributed to the favourable dimer and tetramer hydrogen bonding configurations observed in the two phases. Both of these studies were performed in an inert silicone oil medium which may have helped to supress the conversion into the δ-form from either of these initial phases due to the significant molecular rearrangement required. The change to media in which there is some solubility of *p*ABA may facilitate the transition.

High pressure Neutron diffraction

To follow the single crystal measurements and provide structural information with respect to the compression behaviour we used neutron powder diffraction for phase identification. The advantage of not requiring heat to anneal the solid into a single crystal allowed us to monitor the transition purely with pressure and bypass any effects of temperature. The unit cell parameters of the previously-determined α-polymorph of *p*ABA at 100 K are a = 18.562(1) Å, b = 3.732(<1) Å, c = 18.568(1) Å, β = 93.99(<1)°.[28] The large unit cell made the fitting of the data extremely challenging due to peak overlap in the d-spacing range available on the Pearl instrument however, we were able to obtain a Pawley fit to the data at all pressures (Figure S1). Figure 2 shows the powder diffraction patterns of *p*ABA in the three different solvent compositions on increasing pressure. From these experiments we observe that the behaviour of *p*ABA is different depending on the solvent that is used as the pressure-transmitting medium. The *p*ABA sample in D_2O converts cleanly from α-*p*ABA to δ-*p*ABA (Figure 2a). The conversion to δ-*p*ABA appears to begin at approximately 0.79(8) GPa and is complete by 0.956(10) GPa. The Pawley fits to the ambient pressure data and those collected at 1.104(9) GPa are shown in Figure 3. These refinements show that α-*p*ABA is present from the beginning of the experiment rather the thermodynamically stable β-*p*ABA. The sample at 1.104(9) GPa shows a misfit at 2.5 Å which we attribute to ice VI. The samples in ethanol and water:ethanol show no conversion to δ-*p*ABA on compression (Figure 2b&c). Our original hypothesis that enhanced solubility in the pressure medium facilitates the α- to δ-*p*ABA transition (in part informed by the absence of transformation when using low-solubility silicone oil[36]) cannot be reconciled with our observations here. We believe that the viscosity of the solution may be causing difficulties in molecular mobility hence the nucleation of the high-pressure phase. An increase in viscocity with pressure is observed in pure methanol and 4:1 methanol:ethanol liquid systems and so one can assume that becomes even more significant with

solute present.[51] During loading of the samples, either in the DAC or PE press, there is little control over the quantity of sample and solvent loaded hence no way in which to measure the solubility or supersaturation which can change with pressure.[52] We later followed the same thermodynamic route using optical microscopy study within a DAC offline. For the sample in water α-*p*ABA converts to δ-*p*ABA within 45 minutes at 0.85 GPa which was easily identifed using Raman spectroscopy (Figure 4). This was a similar timespan to that observed in the neutron diffraction experiment. For the 50:50 mixture we observed that over a timespan of 8 hours at 1.35 GPa the conversion of α-*p*ABA into another new phase occurs, which remains unidentified. The Raman spectrum for this sample was collected and shown to be different to the known phases for which we have Raman data (Figure S2). Annealing the powder of the new phase resulted in the formation of δ-*p*ABA coupled with a reduction of pressure to 0.80(5) GPa . At 1.85(5) GPa the α-form persists for 75 hours. We reduced the pressure to 0.99(5) GPa for 24 hours and over this time period the sample did not change and remained as the α-form. We further reduced the pressure to 0.75(5) GPa and we observed that the transition between α-form and δ-form occurs within 7 hours after which the pressure was determined to be 0.64(5) GPa.

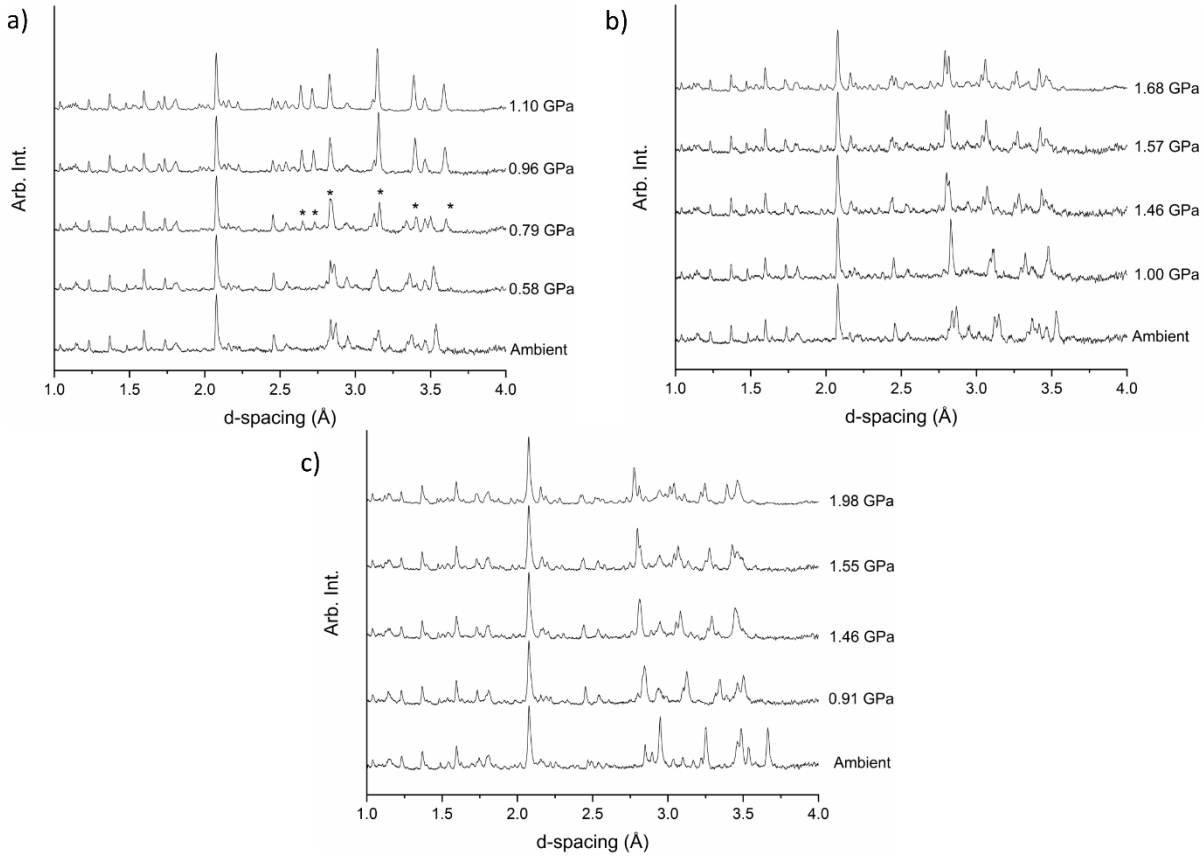

Figure 2: Neutron diffraction data for the compression of *p*ABA-d^4 in (a) water-d^2; b) 50:50 water-d^2:ethanol-d^6 mixture; and c) pure ethanol-d^6. The conversion to the δ-form is complete in the water-d^2 by 0.956(10) GPa whereas the conversion to δ-*p*ABA does not occur in the other two media. Asterisks indicate the peaks of δ-*p*ABA emerging from α-*p*ABA.

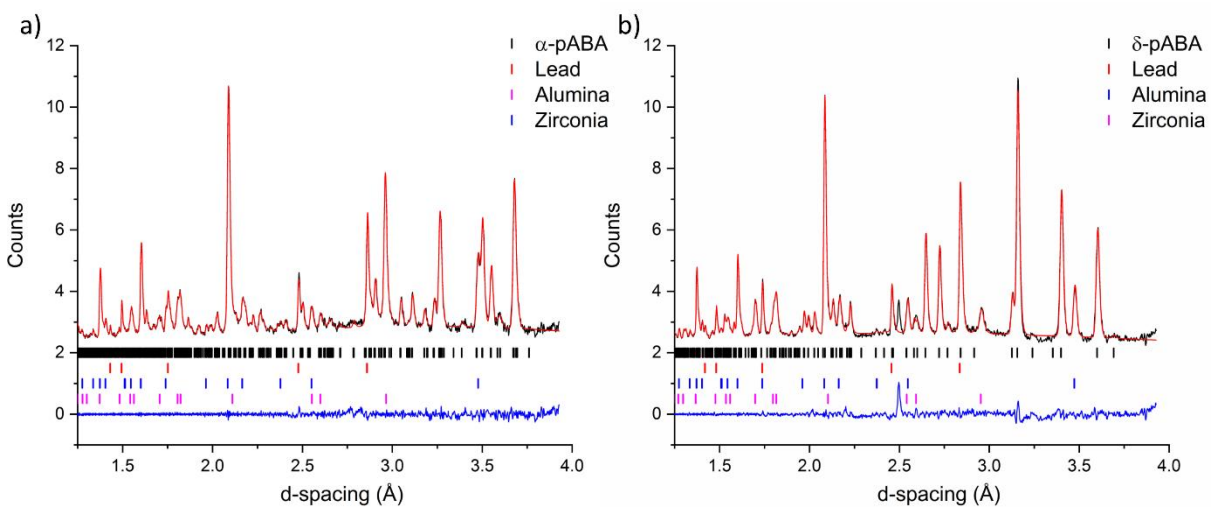

Figure 3 a) The Pawley fit of the α-form to the ambient pressure neutron diffraction dataset of *p*ABA-d^4 in water-d^2. b) The Pawley fit of the δ-form to the ambient pressure neutron diffraction dataset of pABA-d^4 in water-d^2 collected at 1.104(8) GPa. There is a misfit at ~2.5 Å that can be attributed to the (2 1 1) reflection of ice VI.

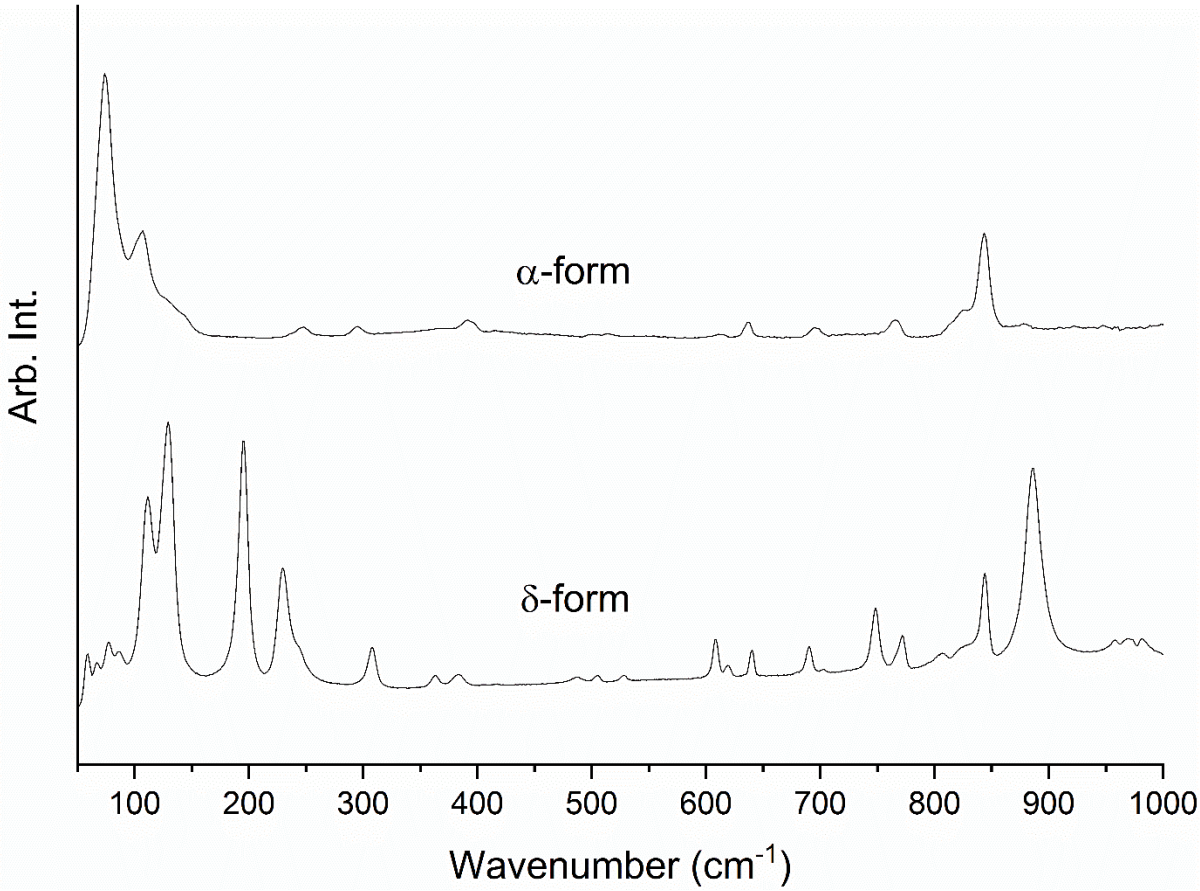

Figure 4: Raman spectra for the α-form and δ-form showing the large difference in the 50-1000 cm^{-1} range.

On decompression to ambient pressure we observe in both the 50:50 water:ethanol and pure ethanol samples that there is conversion to δ-*p*ABA. This begins at 0.638(16) GPa in the mixture whilst it is already complete by 0.376(6) GPa in ethanol (Figure 5). One of the key features is that, in all three cases, δ-*p*ABA is sufficiently stable at ambient pressure for recovery and charaterisation. This is an exciting observation as it is a further example of a material whose high-pressure polymorph is sufficiently stable to be recovered to ambient pressure. A number of other materials have been shown to exhibit this phenomenon, for example γ-amino butyric acid (GABA).H_2O,[16] paracetamol,[53] maleic acid,[53] 3-hydroxy-4,5-dimethyl-1-phenylpyridazin-6-one[54] and glycolide.[24,48] Due to the constraints of allocated measurement time on the Pearl instrument we were only able to monitor the recovered forms for 2 hours however over this time period there was no sign of conversion.

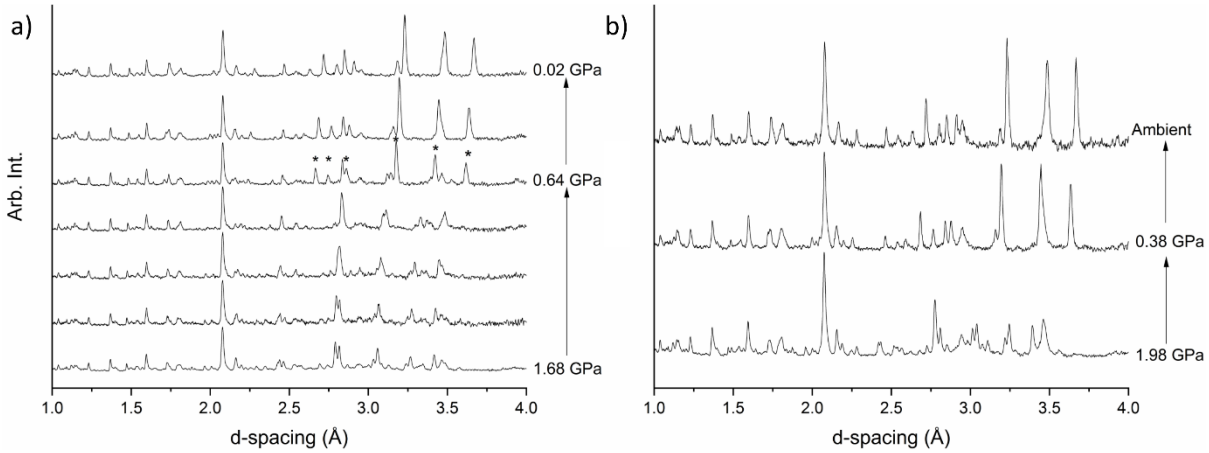

Figure 5: The diffraction patterns of *p*ABA on decompression from the highest pressure achieved in each medium a) 50:50 water-d^2:ethanol-d^6; and b) ethanol-d^6. The α-form transforms cleanly to the δ-form on decompression and persists at ambient pressure. The growth of the δ-form from the α-form is shown by asterisks in a).

Recovery of δ-pABA – Large Volume Press

The ability to analyse material properties *in-situ* at high pressure is challenging but with *p*ABA-h^7 we had the opportunity to recover the high-pressure phase and investigate its properties under ambient pressure. Using the LVP we were able to recreate the conditions of the Pearl experiment but in a much larger quantity (300 mg scale). The maximum pressure generated by the press is 0.8 GPa which is beyond the transition point hence we held α-*p*ABA-h^7 in a saturated aqueous solution at this pressure for 16 hours. On downloading, the recovered sample showed a plate morphology in contrast with the needle-like morphology of α-*p*ABA (Figure 6a); this is consistent with the block morphology observed in the cell where the environment can geometrically constrain the morphology. The unit cell parameters of the δ-form can be fitted to the X-ray diffraction pattern of a sample recovered from the press that has not been ground (Figure 6b). We attempted to collect

capillary data on the sample but it appears that on grinding the powder δ-*p*ABA converts to a mixture of β-*p*ABA and α-*p*ABA (Figure 6c).

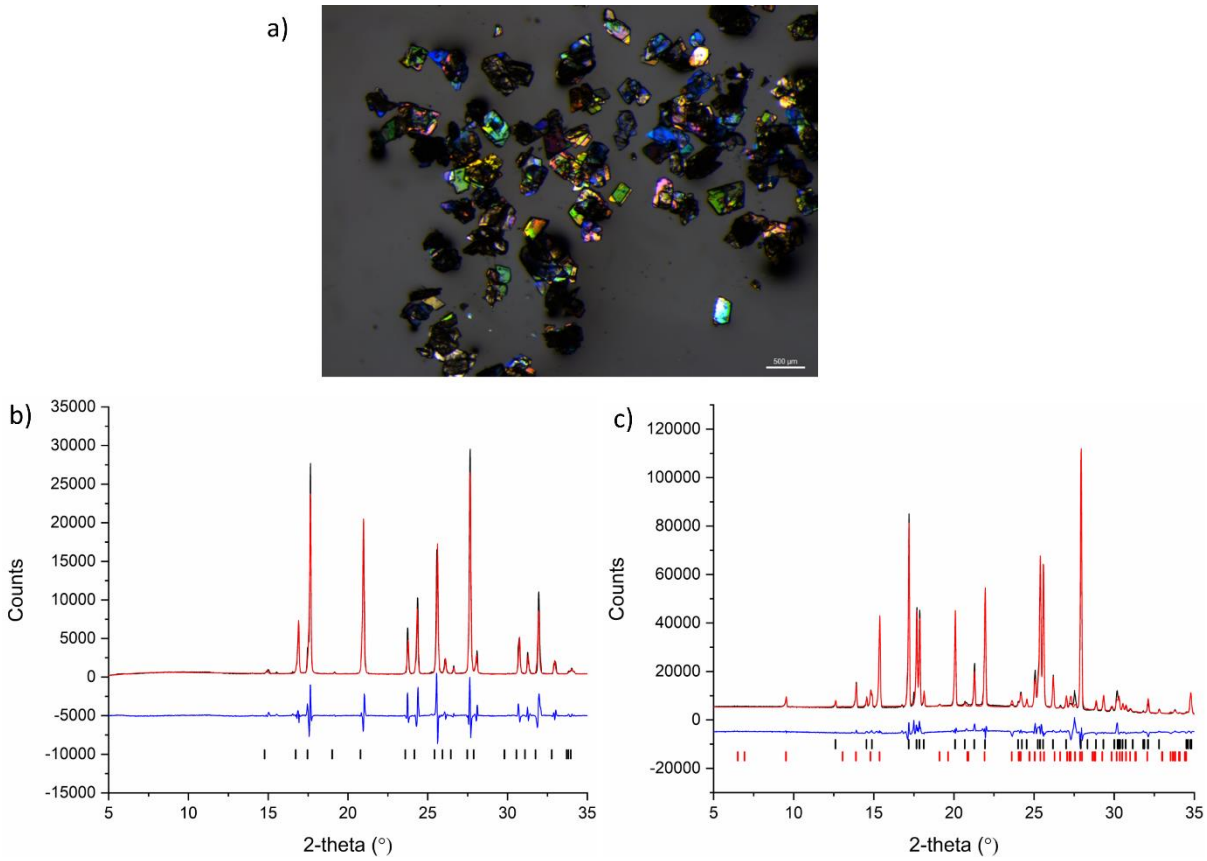

Figure 6: a) Crystals of recovered δ-*p*ABA at ambient pressure. The plate morphology is distinct from the needle and block morphologies of α-*p*ABA and β-*p*ABA. b) The Pawley fit of the recovered δ-*p*ABA without prior grinding. Black tick marks represent the positions of the δ-*p*ABA reflections. c) The Pawley fit of data from collection in a capillary indicating that after 30 minutes and grinding the sample the conversion to a mixture of β-*p*ABA (black ticks) and α-*p*ABA (red ticks) has occurred.

The distinct morphology allowed us to have confidence throughout our analysis that δ-*p*ABA was stable for a matter of weeks as long as we did not grind the powder. Differential scanning calorimetry was performed on the recovered phase and its trace is shown in Figure 7. On heating δ-*p*ABA exhibits a small shallow endotherm (+2 kJ/mol) caused by the reconstructive transition to α-*p*ABA which melts at 187.7ºC. On cooling, the solid nucleates. Subsequent analysis of the solid has identified the solid as the γ-polymorph through use of the IR absorbance bands at 891 and 911 cm^{-1} (Figure S3);[34] these peaks are far more separated in α-*p*ABA (890 and 922 cm^{-1}). The IR analysis and DSC trace leads us to believe that the γ-form is stable until the melt although there

may be the possibility that both γ-*p*ABA and α-*p*ABA are present due to the double peak on melting in the second cycle.

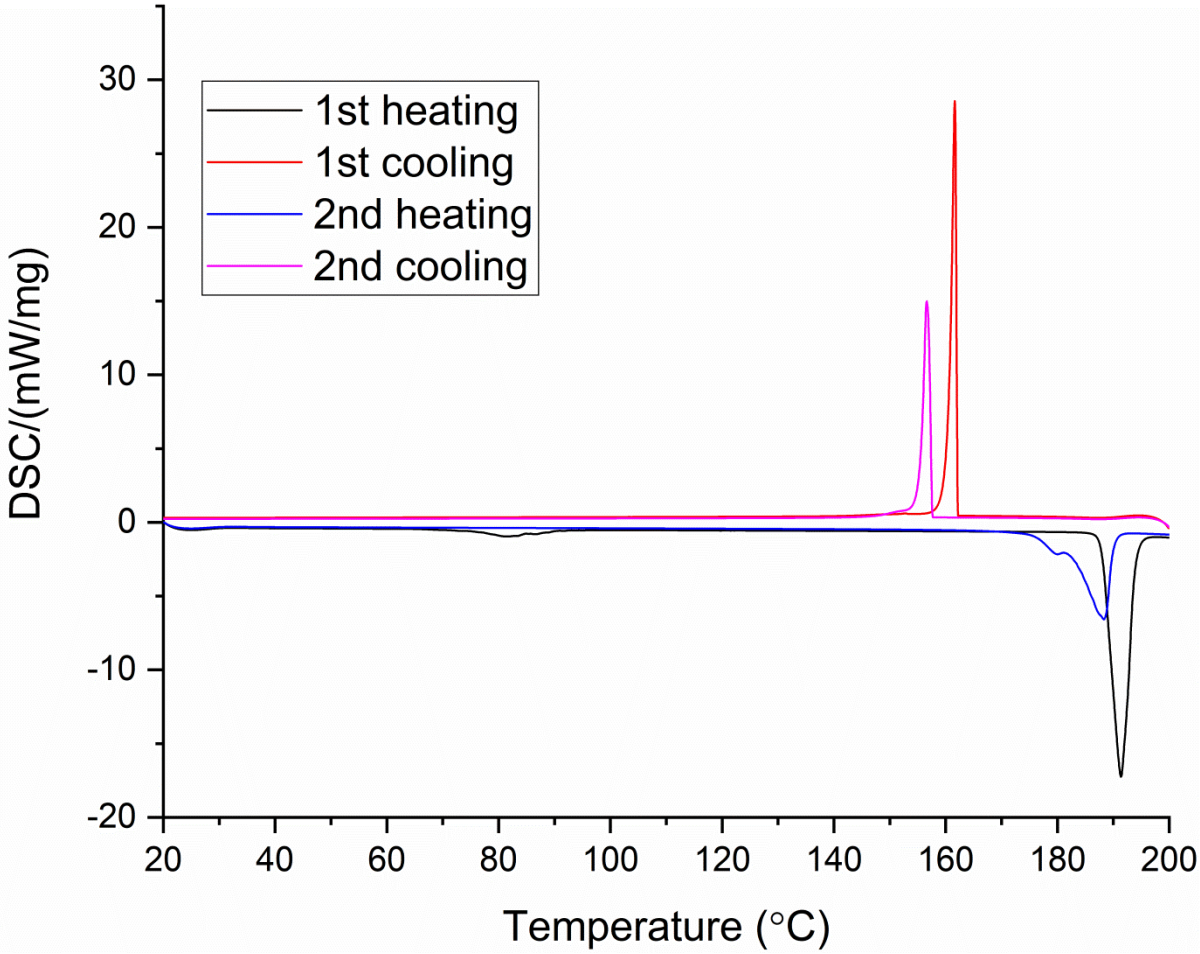

Figure 7: The differential scanning calorimetry trace for δ-*p*ABA. Data were collected at 20°C^{min-1} from 20-200°C. The black trace is the original material from the LVP identified as δ-*p*ABA that undergoes the transition to α-*p*ABA on heating (76°C). The red trace is the cooling of the melt with recrystallisation at ~160°C. The blue trace is the reheating of the recrystallised material which we have identified through IR spectroscopy to be γ-*p*ABA. The pink trace is the cooling of the melt with recrystallisation taking place at 156°C. Note the reduced peak due to some decomposition on melting as well as a change in endotherm shape due to the change in contact between the sample and the base of the pan.

The discovery and recovery of δ-*p*ABA has demonstrated that high pressure can be a powerful tool for the exploration of the solid state. The result presented herein joins a growing list of compounds whose high-pressure polymorphs are recoverable to ambient pressure as a metastable form. Of those polymorphs recovered to ambient pressure there are a number for which high pressure routes are the only method for their production which highlights the potential for pressure as a screening tool for polymorphism. Aminobutyric acid, glycolide, 3-hydroxy-4,5-

dimethyl-1-phenylpyridazin-6-one and paracetamol form novel, recoverable phases that have not been observed at ambient pressure despite many crystallisation experiments. Fabbiani and co-workers were able to demonstrate the recovery of γ-aminobutyric acid monohydrate to ambient pressure.[55] In this case, pressure was applied to 4 M solutions of aminobutyric acid and through pressure precipitation the hydrate was observed at 0.44 GPa. The authors were able to decompress the hydrate and use the crystal to seed ambient pressure solutions. The key observation in this work was that the high-pressure precipitation method was the only way in which to observe the hydrated form despite an extensive screen of crystallisation conditions. Seeding was also possible in the case of glycolide. Our group has recovered a new high-pressure polymorph of glycolide in large quantities (300mg). Using the LVP we were able to isolate and recover the high-pressure form to ambient pressure and use these crystals as seeds for crystallisation experiments to obtain single crystal for identification; the high pressure form was stable for up to 12 days.[48]

Pressure-preciptiation was the sole route for the isolation of the γ-polymorph of 3-hydroxy-4,5-dimethyl-1-phenylpyridazin-6-one. Roszak et al[54] discovered that the high-pressure phase (γ-form) could only be isolated at high pressure despite the polymorph showing extensive metastability (over a year) in open vials on the bench at ambient pressure. The authors did not state whether seeding experiments were performed on these materials. One key observation of the structure was the high energy molecular conformation adopted by the molecules in the γ-form (forced by efficient packing) may have prevented isolation through ambient pressure routes.

Finally, Oswald et al. have demonstrated that the metastable orthorhombic polymorph of paracetamol can be succesfully isolated to ambient pressure using a variety of concentrations.[53] The stability of the orthorhombic form was altered depending on the concentration of solutions used for the precipitation experiment. At >140mg/ml of paracetmol in water the authors demonstrated that the solid converts to the monoclinic form over the course of several hours but that the conversion can be retarded by cooling to 275-280 K. A sample at 100mg/ml was stable for a period of days and provided crystals satisfactory for single crystal X-ray analysis. With concentrations <100 mg/ml the monohydrate of paracetamol was obtained (sole route to isolation) and recovered. In both cases, the crystals recovered from high pressure could be used as seed crystals.

In each of these examples in the literature and the present one in this study, the discovery and isolation of these forms has been serendipitous hence there is a strong need to be able to develop strategies to identify materials that are likely to i) undergo a transition to a new form; and ii) be recoverable to ambient pressure. Only once these strategies have been developed can high-pressure precipitation be a robust tool for industry as a polymorph screening methodology.

In conclusion, we have shown that *p*ABA undergoes a phase transformation at high pressure from α-*p*ABA to a new polymorph that we have designated δ-*p*ABA. Through precipitation from solution we have identified that the pressure of the phase transition is relatively low at ~0.3 GPa. We have observed that whilst having low solubility in water the phase transformation takes place easily over a short timescale (45 mins). In solvents in which *p*ABA is more soluble (e.g. ethanol) the transition is hindered (8 hours) but it is accelerated by decompression of the solution to ambient pressure. Molecular mobility in the solvent media is cited as a possible explanation for this. The high-pressure δ-*p*ABA is recoverable to ambient pressure as a metastable form and converts to α- and β-*p*ABA on grinding at room temperature (20-25°C); heating converts δ-*p*ABA to α-*p*ABA .

Acknowledgements

The authors would like to thank Roger Davey of University of Manchester for useful discussions and Lloyd Farquahar for help during beamtime. We would like to thank Science and Technology Facilites Council for the award of beamtime (RB1810710).[56] ACC would like to acknowlege the Royal Society for an Industry Fellowship in Astra Zeneca and IDHO & MRW thank the EPSRC for funding (EP/N015401-1). All data underpinning this publication are openly available from the University of Strathclyde KnowledgeBase at XXX (to be validated once article is accepted). CCDC deposition numbers are 1876686-1876690.

References

1 J. Bernstein, *Cryst. Growth Des.*, 2011, **11**, 632–650.

2 J. Bauer, S. Spanton, R. Henry, J. Quick, W. Dziki, W. Porter and J. Morris, *Pharm. Res.*, 2001, **18**, 859–66.

3 A. Fouskova, O. Sedmik and V. Svoboda, *Ceskoslov. Cas. Pro Fys. Sekce a*, 1971, **21**, 275-.

4 F. Smutný, *Phys. Status Solidi*, 1972, **9**, K109–K110.

5 J. Cosier, A. M. Glazer and IUCr, *J. Appl. Crystallogr.*, 1986, **19**, 105–107.

6 Y. V Seryotkin, T. N. Drebushchak and E. V Boldyreva, *Acta Crystallogr. Sect. B*, 2013, **69**, 77–85.

7 B. A. Zakharov, Y. V Seryotkin, N. A. Tumanov, D. Paliwoda, M. Hanfland, A. V Kurnosov and E. V Boldyreva, *RSC Adv.*, 2016, **6**, 92629–92637.

8 E. Patyk, J. Skumiel, M. Podsiadlo and A. Katrusiak, *Angew. Chemie-International Ed.*, 2012, **51**, 2146–2150.

9 R. Lee, D. S. Yufit, M. R. Probert and J. W. Steed, *Cryst. Growth Des.*, 2017, **17**, 1647–1653.

10 D. I. A. Millar, H. E. Maynard-Casely, A. K. Kleppe, W. G. Marshall, C. R. Pulham and A. S. Cumming, *CrystEngComm*, 2010, **12**, 2524–2527.

11 N. Abbas, I. Oswald and C. Pulham, *Pharmaceutics*, 2017, **9**, 16.

12 S. A. Moggach, W. G. Marshall and S. Parsons, *Acta Crystallogr. Sect. B Struct. Sci.*, 2006, **62**, 815–825.

13 C. L. Bull, G. Flowitt-Hill, S. de Gironcoli, E. Küçükbenli, S. Parsons, C. Huy Pham, H. Y. Playford and M. G. Tucker, 2017, **4**, 569–574.

14 I. D. H. Oswald and C. R. Pulham, *CrystEngComm*, 2008, **10**, 1114–1116.

15 F. P. A. Fabbiani, G. Buth, B. Dittrich and H. Sowa, *CrystEngComm*, 2010, **12**, 2541.

16 F. P. A. Fabbiani, G. Buth, D. C. Levendis and A. J. Cruz-Cabeza, *Chem. Commun. (Camb).*, 2014, **50**, 1817–9.

17 L. E. Connor, C. A. Morrison, I. D. H. Oswald, C. R. Pulham and M. R. Warren, *Chem. Sci.*, , DOI:10.1039/c7sc01379e.

18 I. D. H. Oswald, A. R. Lennie, C. R. Pulham and K. Shankland, *CrystEngComm*, 2010, **12**, 2533.

19 A. Delori, I. B. Hutchison, C. L. Bull, N. P. Funnell, A. J. Urquhart and I. D. H. Oswald, *Cryst. Growth Des.*, 2018, **18**, 1425–1431.

20 B. A. Zakharov and E. V Boldyreva, *J. Mol. Struct.*, 2014, **1078**, 151–157.

21 S. Bergantin, M. Moret, G. Buth and F. P. A. Fabbiani, *J. Phys. Chem. C*, 2014, **118**, 13476–13483.

22 B. A. Zakharov, E. A. Losev and E. V Boldyreva, *CrystEngComm*, 2013, **15**, 1693.

23 N. P. Funnell, W. G. Marshall and S. Parsons, *CrystEngComm*, 2011, **13**, 5841–5848.

24 I. B. Hutchison, C. L. Bull, W. G. Marshall, S. Parsons, A. J. Urquhart and I. D. H. Oswald, *Acta Crystallogr. Sect. B Struct. Sci. Cryst. Eng. Mater.*, 2017, **73**, 1151–1157.

25 S. Li, Q. Li, J. Zhou, R. Wang, Z. Jiang, K. Wang, D. Xu, J. Liu, B. Liu, G. Zou and B. Zou, *J. Phys. Chem. B*, 2012, **116**, 3092–3098.

26 A. Y. Fedorov, D. A. Rychkov, E. A. Losev, B. A. Zakharov, J. Stare and E. V. Boldyreva, *CrystEngComm*, 2017, **19**, 2243–2252.

27 R. A. Sullivan, R. J. Davey, G. Sadiq, G. Dent, K. R. Back, J. H. ter Horst, D. Toroz and R. B. Hammond, *Cryst. Growth Des.*, 2014, **14**, 2689–2696.

28 R. A. Sullivan and R. J. Davey, *CrystEngComm*, 2015, **17**, 1015–1023.

29 S. Gracin and Å. C. Rasmuson, *Cryst. Growth Des.*, 2004, **4**, 1013–1023.

30 M. Svard, F. L. Nordstrom, E. M. Hoffmann, B. Aziz and A. C. Rasmuson, *Crystengcomm*, 2013, **15**, 5020–5031.

31 R. C. G. Killean, P. Tollin, D. G. Watson, D. W. Young and IUCr, *Acta Crystallogr.*, 1965, **19**, 482–483.

32 R. Benali-Cherif, R. Takouachet, E.-E. Bendeif, N. Benali-Cherif and IUCr, *Acta Crystallogr. Sect. C Struct. Chem.*, 2014, **70**, 323–325.

33 N. Kamali, C. O'Malley, M. F. Mahon, A. Erxleben and P. McArdle, *Cryst. Growth Des.*, 2018, **18**, 3510–3516.

34 N. Kamali, A. Erxleben and P. McArdle, *Cryst. Growth Des.*, 2016, **16**, 2492–2495.

35 S. Athimoolam, S. Natarajan and IUCr, *Acta Crystallogr. Sect. C Cryst. Struct. Commun.*, 2007, **63**, o514–o517.

36 T. Yan, K. Wang, D. Duan, X. Tan, B. Liu and B. Zou, *RSC Adv.*, 2014, **4**, 15534–15541.

37 S. A. Moggach, D. R. Allan, S. Parsons and J. E. Warren, *J. Appl. Crystallogr.*, 2008, **41**, 249–251.

38 G. J. Piermarini, S. Block, J. D. Barnett and R. A. Forman, *J. Appl. Phys.*, 1975, **46**, 2774–2780.

39 G. J. Piermarini, S. Block, J. D. Barnett and R. a. Forman, *J. Appl. Phys.*, 1975, **46**, 2774–2780.

40 G. M. Sheldrick, *SADABS, Programs Scaling Absorpt. Correct. Area Detect. Data*, 2008, University of Göttingen: Göttingen, Germany.

41 J. Cosier and A. M. Glazer, *J. Appl. Crystallogr.*, 1986, **19**, 105–107.

42 G. M. Sheldrick and IUCr, *Acta Crystallogr. Sect. A Found. Adv.*, 2015, **71**, 3–8.

43 O. V. Dolomanov, L. J. Bourhis, R. J. Gildea, J. A. K. Howard, H. Puschmann and IUCr, *J. Appl. Crystallogr.*, 2009, **42**, 339–341.

44 A. Dawson, D. R. Allan, S. Parsons and M. Ruf, *J. Appl. Crystallogr.*, 2004, **37**, 410–416.

45 C. L. Bull, N. P. Funnell, M. G. Tucker, S. Hull, D. J. Francis and W. G. Marshall, *High Press. Res.*, 2016, **36**, 493–511.

46 P. Taylor, M. Street, L. Wt, D. I. A. Millar, W. G. Marshall, I. D. H. Oswald, C. R. Pulham, I. A. David, G. William, D. H. Iain and C. R. High-, *Crystallogr. Rev.*, 2010, **16**, 115–132.

47 O. Arnold, J. C. Bilheux, J. M. Borreguero, A. Buts, S. I. Campbell, L. Chapon, M. Doucet, N. Draper, R. Ferraz Leal, M. A. Gigg, V. E. Lynch, A. Markvardsen, D. J. Mikkelson, R. L. Mikkelson, R. Miller, K. Palmen, P. Parker, G. Passos, T. G. Perring, P. F. Peterson, S. Ren, M. A. Reuter, A. T. Savici, J. W. Taylor, R. J. Taylor, R. Tolchenov, W. Zhou and J. Zikovsky, *Nucl. Instruments Methods Phys. Res. Sect. A Accel. Spectrometers, Detect. Assoc. Equip.*, 2014, **764**, 156–166.

48 I. B. Hutchison, A. Delori, X. Wang, K. V. Kamenev, A. J. Urquhart and I. D. H. Oswald, *CrystEngComm*, 2015, **17**, 1778–1782.

49 F. P. A. Fabbiani and C. R. Pulham, *Chem. Soc. Rev.*, 2006, **35**, 932.

50 F. P. A. Fabbiani, D. R. Allan, A. Dawson, W. I. F. David, P. A. McGregor, I. D. H. Oswald, S. Parsons and C. R. Pulham, *Chem. Commun. (Camb).*, 2003, 3004–3005.

51 B. Grocholski and R. Jeanloz, *J. Chem. Phys.*, 2005, **123**, 204503.

52 N. T. Morgan, T. C. Frank, R. J. Holmes and E. L. Cussler, *Cryst. Growth Des.*, 2016, **16**, 1404–1408.

53 I. D. H. Oswald, I. Chataigner, S. Elphick, F. P. A. Fabbiani, A. R. Lennie, J. Maddaluno, W. G. Marshall, T. J. Prior, C. R. Pulham and R. I. Smith, *CrystEngComm*, 2009, **11**, 359–366.

54 K. Roszak, A. Katrusiek and A. Katrusiak, *Cryst. Growth Des.*, 2016, **16**, 3947–3953.

55 F. P. A. Fabbiani, G. Buth, D. C. Levendis and A. J. Cruz-Cabeza, *Chem. Commun.*, 2014, **50**, 1817–1819.

56 I. D. H. Oswald, A. J. Cruz-Cabeza, C. L. Bull, M. R. Ward and L. Farquhar, Effect of pressure-transmitting medium on the phase transformation of para-aminobenzoic acid., https://data.isis.stfc.ac.uk/doi/investigation/90588565.

Supplementary Information - Discovery and Recovery of delta *p*-aminobenzoic acid

Martin R. Ward,[1] Shatha Younis,[1] Aurora J. Cruz-Cabeza,[2] Craig L. Bull,[3] Nicholas P. Funnell,[3] and Iain D.H. Oswald[1]

[1] Strathclyde Institute of Pharmacy & Biomedical Sciences (SIPBS), University of Strathclyde, 161 Cathedral Street, G4 0RE, Glasgow, U.K.

[2] School of Chemical Engineering and Analytical Science, University of Manchester, M13 9PL Manchester, United Kingdom

[3] ISIS Neutron and Muon Source, Science and Technology Facilities Council, Rutherford Appleton Laboratory, Harwell, Didcot, OX11 0QX, UK

Table S1. Experimental details

For all structures: $C_7H_7NO_2$, M_r = 137.14, monoclinic, *Pn*, *Z* = 2. Refinement was with 71 restraints.

	δ-*p*ABA recovered from high pressure	δ-*p*ABA recovered from high pressure	δ-*p*ABA in ethanol at 0.49 GPa	δ-*p*ABA in water at 0.33 GPa
Crystal data				
Temperature (K)	295	100	296	296
a, *b*, *c* (Å)	6.5086 (5), 4.6661 (4), 10.7596 (8)	6.4551 (5), 4.6740 (4), 10.5470 (9)	6.4341 (11), 4.6151 (3), 10.5313 (7)	6.4342 (10), 4.6146 (4), 10.5397 (10)
β (°)	100.685 (1)	100.754 (3)	100.73 (1)	100.667 (9)
V (Å^3)	321.10 (4)	312.63 (4)	307.25 (6)	307.53 (6)
Radiation type	Mo *K*α	Cu *K*α	Mo *K*α	Mo *K*α
μ (mm^{-1})	0.11	0.91	0.11	0.11
Crystal size (mm)	0.2 × 0.15 × 0.02	0.2 × 0.18 × 0.02	0.15 × 0.08 × 0.08	0.15 × 0.08 × 0.05
Data collection				
Diffractometer	Bruker *APEX*-II CCD	Bruker *APEX*-II CCD	Bruker *SMART APEX2* area detector	Bruker *SMART APEX2* area detector
Absorption correction	Multi-scan *SADABS2016*/2 (Bruker,2016/2) was used for absorption correction. wR2(int) was 0.1202 before and 0.0619 after correction. The Ratio of minimum to maximum transmission is 0.8072. The λ/2 correction factor is Not present.	Multi-scan *SADABS2016*/2 (Bruker,2016/2) was used for absorption correction. wR2(int) was 0.0715 before and 0.0460 after correction. The Ratio of minimum to maximum transmission is 0.8525. The λ/2 correction factor is Not present.	Multi-scan *SADABS2016*/2 (Bruker,2016/2) was used for absorption correction. wR2(int) was 0.0921 before and 0.0409 after correction. The Ratio of minimum to maximum transmission is 0.9017. The λ/2 correction factor is Not present.	Multi-scan *SADABS2016*/2 (Bruker,2016/2) was used for absorption correction. wR2(int) was 0.1150 before and 0.0458 after correction. The Ratio of minimum to maximum transmission is 0.8491. The λ/2 correction factor is Not present.
T_{min}, T_{max}	0.603, 0.746	0.643, 0.754	0.672, 0.745	0.633, 0.745
No. of measured, independent and observed [$I > 2\sigma(I)$] reflections	7461, 2326, 2079	3384, 1014, 991	1365, 357, 320	1444, 471, 396
R_{int}	0.040	0.035	0.030	0.043
θ_{max} (°)	32.6	74.2	23.3	23.2
$(\sin\theta/\lambda)_{max}$ (Å^{-1})	0.758	0.624	0.556	0.554

Refinement				
$R[F^2 > 2\sigma(F^2)]$, $wR(F^2)$, S	0.041, 0.115, 1.05	0.029, 0.073, 1.11	0.034, 0.077, 1.17	0.041, 0.107, 1.11
No. of reflections	2326	1014	357	471
No. of parameters	93	100	81	81
H-atom treatment	H-atom parameters constrained	H atoms treated by a mixture of independent and constrained refinement	H-atom parameters constrained	H-atom parameters constrained
$\Delta\rho_{max}$, $\Delta\rho_{min}$ (e Å^{-3})	0.27, -0.19	0.18, -0.24	0.11, -0.10	0.16, -0.16
Absolute structure	Flack x determined using 955 quotients [(I+)-(I-)]/[(I+)+(I-)] (Parsons, Flack and Wagner, Acta Cryst. B69 (2013) 249-259).	Flack x determined using 350 quotients [(I+)-(I-)]/[(I+)+(I-)] (Parsons, Flack and Wagner, Acta Cryst. B69 (2013) 249-259).	Flack x determined using 130 quotients [(I+)-(I-)]/[(I+)+(I-)] (Parsons, Flack and Wagner, Acta Cryst. B69 (2013) 249-259).	Flack x determined using 156 quotients [(I+)-(I-)]/[(I+)+(I-)] (Parsons, Flack and Wagner, Acta Cryst. B69 (2013) 249-259).
Absolute structure parameter	-0.4 (6)	0.01 (12)	-0.6 (10)	1.3 (10)

	δ-*p*ABA in 50:50 ethanol:water at 0.8 GPa
Crystal data	
Temperature (K)	295
a, *b*, *c* (Å)	6.4003 (11), 4.5981 (4), 10.4452 (15)
β (°)	100.748 (14)
V (Å^3)	302.00 (7)
Radiation type	Mo *K*α
μ (mm^{-1})	0.11
Crystal size (mm)	0.2 × 0.15 × 0.02
Data collection	
Diffractometer	Bruker *SMART APEX2* area detector
Absorption correction	Multi-scan *SADABS2016*/2 (Bruker,2016/2) was used for absorption correction. wR2(int) was 0.0951 before and 0.0476 after correction. The Ratio of minimum to maximum transmission is 0.7098. The λ/2 correction factor is Not present.
T_{min}, T_{max}	0.529, 0.745
No. of measured, independent and observed [$I > 2\sigma(I)$] reflections	1317, 333, 300

R_{int}	0.030
θ_{max} (°)	23.3
$(\sin \theta/\lambda)_{max}$ (Å^{-1})	0.555
Refinement	
$R[F^2 > 2\sigma(F^2)]$, $wR(F^2)$, S	0.028, 0.064, 1.04
No. of reflections	333
No. of parameters	81
H-atom treatment	H-atom parameters constrained
$\Delta\rho_{max}$, $\Delta\rho_{min}$ (e Å^{-3})	0.09, -0.07
Absolute structure	Flack x determined using 129 quotients [(I+)-(I-)]/[(I+)+(I-)] (Parsons, Flack and Wagner, Acta Cryst. B69 (2013) 249-259).
Absolute structure parameter	1.5 (10)

Computer programs: *SAINT* v8.37A (Bruker, 2015), XT (Sheldrick, 2015), XL (Sheldrick, 2008), Olex2 (Dolomanov *et al.*, 2009).

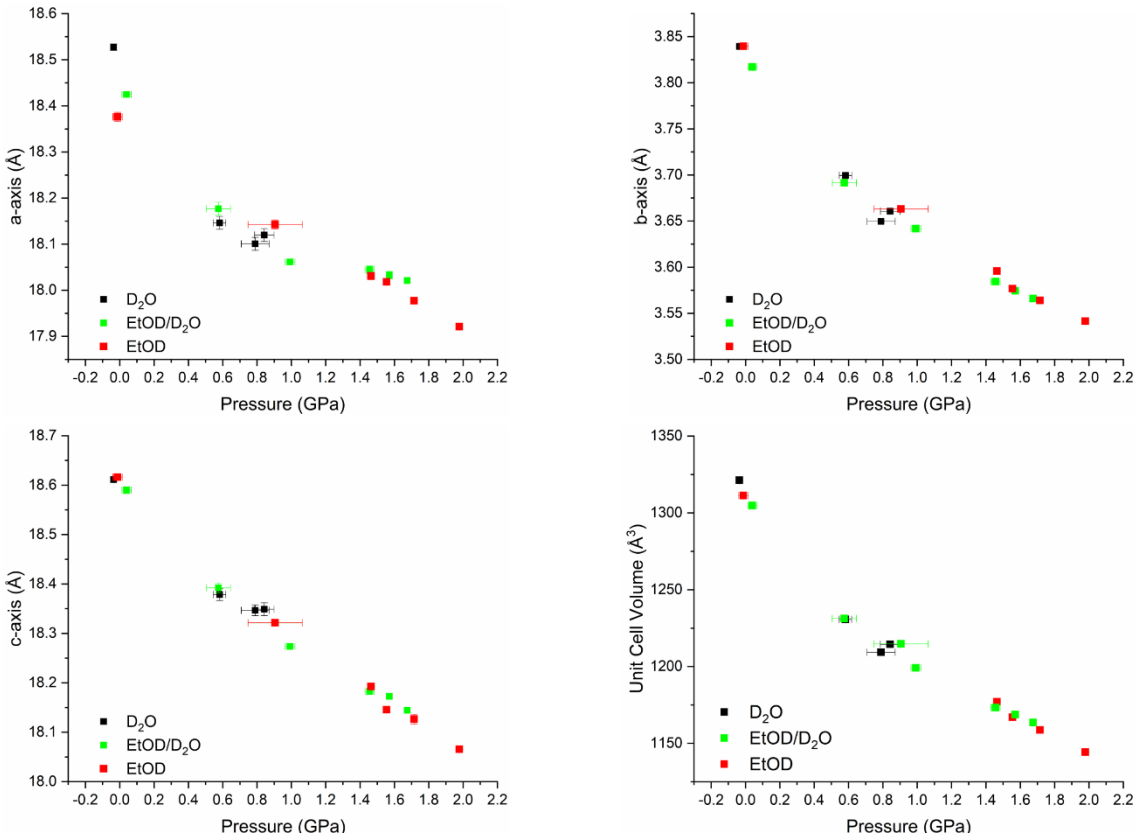

Figure S1: The refined unit cell parameters for α-form as a function of pressure. The parameters are consistent with one another from each of the media.

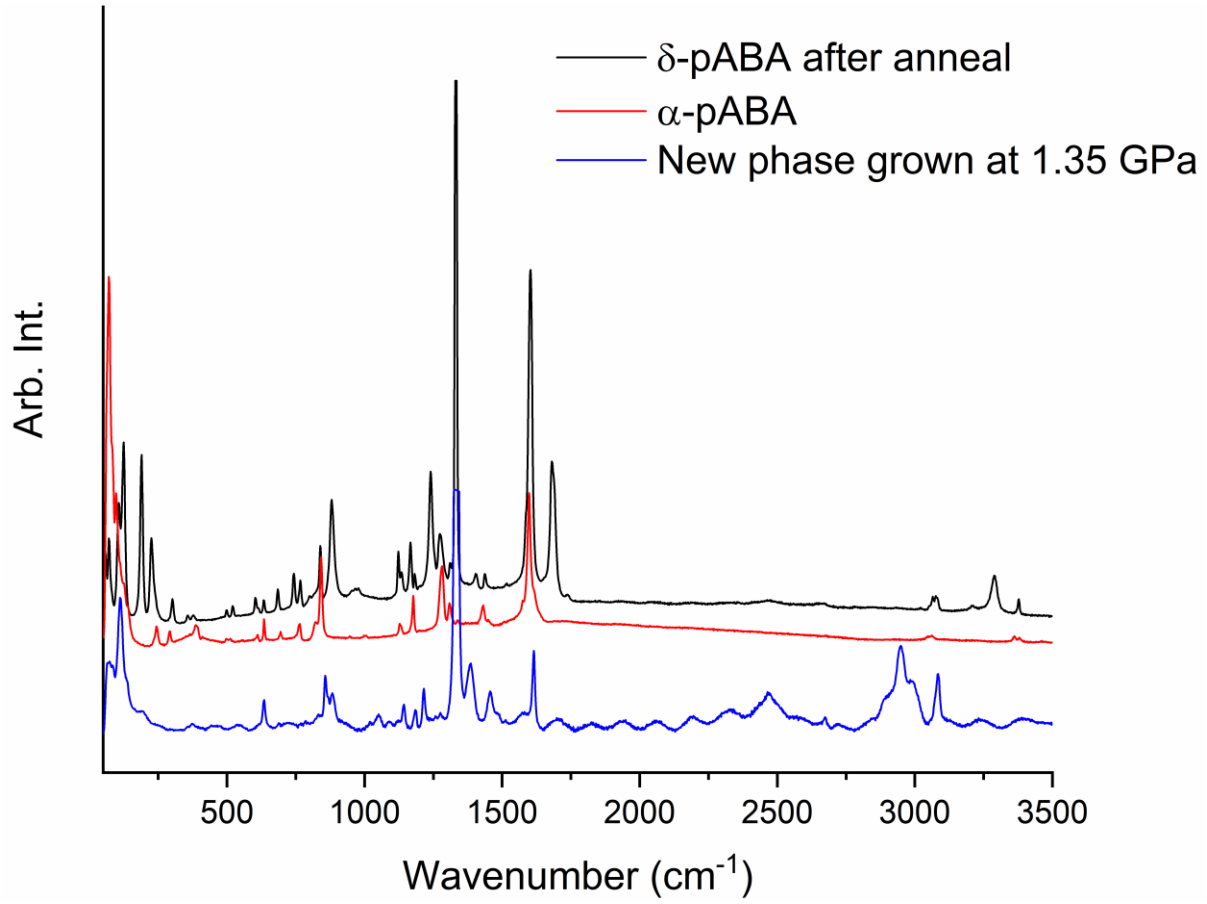

Figure S2: The Raman spectrum for the new phase that nucleated after 8 hours from a α-*p*ABA sample in 50:50 v/v water:ethanol at 1.35 GPa together with the spectrum for α-*p*ABA and the annealed sample which was identified at δ-*p*ABA by single crystal diffraction.

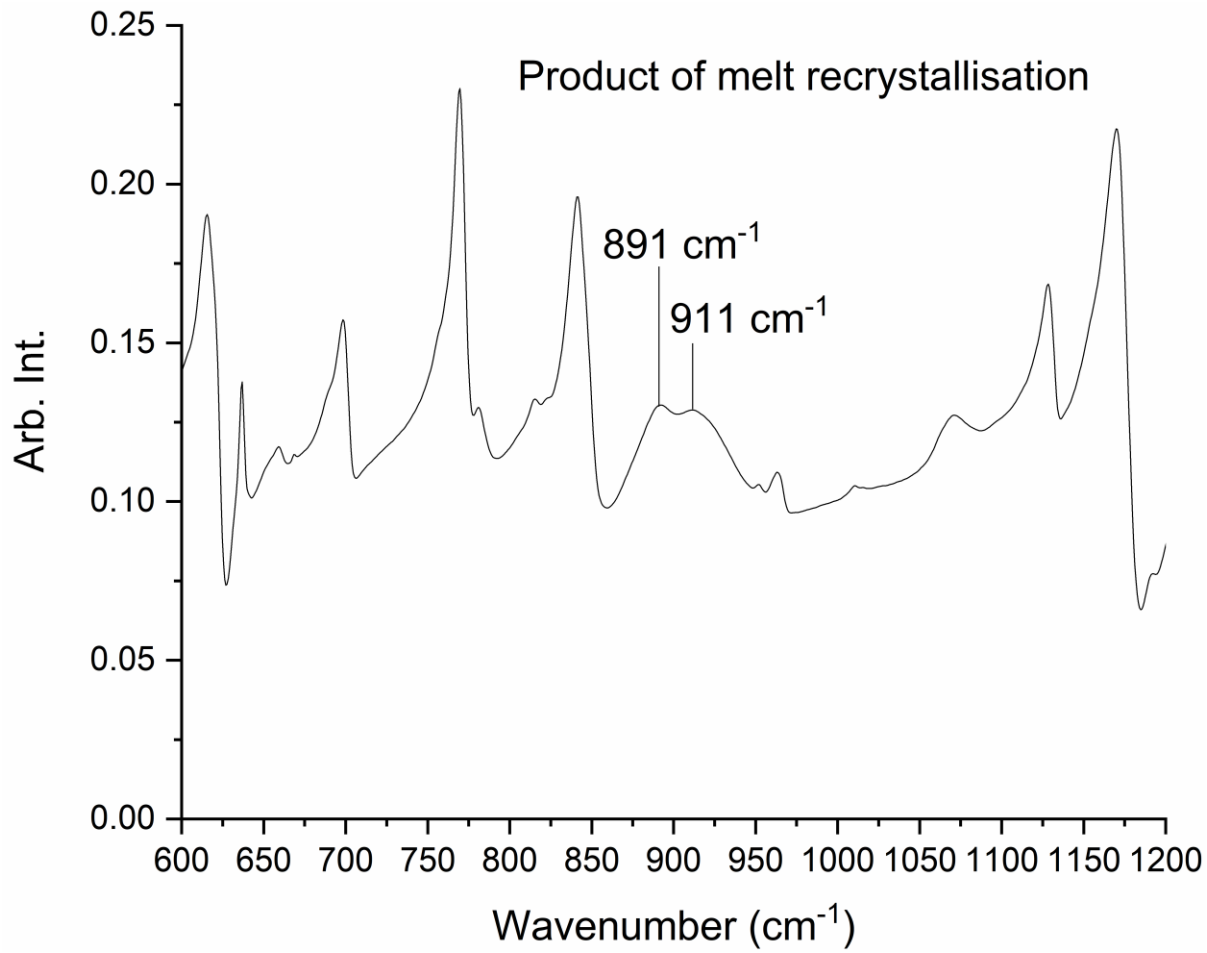

Figure S3: The FT-IR of the recrystallised material from the melt using the DSC sample. The peaks indicate that it is γ-*p*ABA.